2019

Accurate magneto-optical determination of radius of topological nodal-ring semimetals

Wenye Duan
University of Wollongong, wduan@uow.edu.au

Cuihong Yang
University of Wollongong, Nanjing University of Information Science and Technology, cuihong@uow.edu.au

Zhongshui Ma
Chinese Academy Of Sciences, Peking University, Collaborative Innovation Center Of Quantum Matter, zma@uow.edu.au

Yiming Zhu
University of Shanghai For Science And Technology

C Zhang
University of Wollongong, czhang@uow.edu.au

Accurate magneto-optical determination of radius of topological nodal-ring semimetals

Abstract

The shape of the Fermi surface of topological nodal-ring semimetals at low carrier concentrations is characterized by the ring radius b/$\hbar$vF. This peculiar topological property may not have a clear signature in measurable physical quantities. We demonstrate an accurate and definitive method to determine the radius of topological nodal-ring semimetals. Under a magnetic field along the ring axis, the axial magneto-optical response (σ_{zz}) has a giant peak. The position of this ultrastrong response is at the frequency of exactly 2b and is independent of the strength of the magnetic field. The amplitude of the peak response is many times stronger than that of any other inter-Landau level transitions if the magnetic energy is greater than b and is similar strength if b is greater than the magnetic energy. The origin of the ultrastrong response is that the axial magnetic transition is governed by selection rules completely different to those governing σ_{xx} where the giant response is absent [R. Y. Chen et al., Phys. Rev. Lett. 115, 176404 (2015)]. The present work provides a method to accurately determine parameters of the topological properties of semimetals.

Disciplines

Engineering | Science and Technology Studies

Publication Details

Duan, W., Yang, C., Ma, Z., Zhu, Y. & Zhang, C. (2019). Accurate magneto-optical determination of radius of topological nodal-ring semimetals. Physical Review B, 99 (4), 045124-1-045124-6.

Accurate magneto-optical determination of radius of topological nodal-ring semimetals

Wenye Duan,[1] Cuihong Yang,[1,2] Zhongshui Ma,[3,4] Yiming Zhu,[5] and Chao Zhang[1,5,*]

[1]*School of Physics, University of Wollongong, New South Wales 2522, Australia*

[2]*School of Physics and Optoelectronic Engineering, Nanjing University of Information Science and Technology, Nanjing 210044, China*

[3]*School of Physics, Peking University, Beijing 100871, China*

[4]*Collaborative Innovation Center of Quantum Matter, Beijing, 100871, China*

[5]*Terahertz Science Cooperative Innovation Center, University of Shanghai for Science and Technology, Shanghai 200093, China*

(Received 14 September 2018; published 14 January 2019)

The shape of the Fermi surface of topological nodal-ring semimetals at low carrier concentrations is characterized by the ring radius $b/\hbar v_F$. This peculiar topological property may not have a clear signature in measurable physical quantities. We demonstrate an accurate and definitive method to determine the radius of topological nodal-ring semimetals. Under a magnetic field along the ring axis, the axial magneto-optical response (σ_{zz}) has a giant peak. The position of this ultrastrong response is at the frequency of exactly $2b$ and is independent of the strength of the magnetic field. The amplitude of the peak response is many times stronger than that of any other inter-Landau level transitions if the magnetic energy is greater than b and is similar strength if b is greater than the magnetic energy. The origin of the ultrastrong response is that the axial magnetic transition is governed by selection rules completely different to those governing σ_{xx} where the giant response is absent [R. Y. Chen *et al.*, Phys. Rev. Lett. **115**, 176404 (2015)]. The present work provides a method to accurately determine parameters of the topological properties of semimetals.

DOI: 10.1103/PhysRevB.99.045124

I. INTRODUCTION

Recently a new class of topological materials, so-called topological nodal-ring semimetals (TNRSMs), has been predicted [1,2]. Some material candidates are discovered [3,4]. The basic characteristic of the TNRSM is that their conduction and valence bands cross on a closed ring in reciprocal space nonaccidentally [2–12]. These nodal rings are found to be protected by inversion and time reversal symmetries [11–13], by mirror reflection symmetry [10–12,14], and by nonsymmorphic symmetries [9–13]. Owing to their potential applications, many theoretical models for realizing TNRSMs have been proposed [9,12]. The properties of TNRSMs have been investigated, such as the magnetic susceptibility [15], the quantum oscillations [16–21], the Landau quantization [22,23], the quantum anomalies [24], the Lifshitz transitions [25], and other transport properties [26–34] . Electronic correlations and superconductivity have also been studied [35–41].

The topological materials are described by their band structures and are characterized by several key topologically unique parameters. In the Weyl semimetals, it is the distance between the Weyl nodes with different chirality ($|\Delta\mathbf{k}|$). In the TNRSMs, the radius of the ring $b/\hbar v_F$ represents the unique topological properties. In practice, apart from the angle-resolved photoemission spectroscopy, direct physical property measurement of $|\Delta\mathbf{k}|$ or $b/\hbar v_F$ is desirable [3,4,42]. In the case of Weyl semimetals, the chiral anomaly gives rise to an electromagnetic response term of $\mathbf{J} = (e^2/2\pi h)[(\Delta\mathbf{k}) \times \mathbf{E} - (\Delta\varepsilon)\mathbf{B}]$, where $\Delta\varepsilon$ is the energy difference between the Weyl nodes. The first term represents the anomalous Hall effect that is expected to occur in the Weyl semimetals with broken time reversal symmetry [8,43]. Therefore, $|\Delta\mathbf{k}|$ can be determined by the anomalous Hall effect in the Weyl semimetals. However, there is no such simple term for TNRSMs, which is solely determined by the radius of ring $b/\hbar v_F$. In more complicated setups, some physical quantities can be related to b. For example, by using a toroidal field [23], the quantized Hall conductivities are proportional to b. Besides, the orbital magnetization of the sample is also dependent on the ring radius [27]. In this work we shall propose a simple transport parameter which can be used to accurately determine b. The magnetic field required in the present case can be arbitrarily weak.

Recent work on the optical conductivity provided valuable information in Dirac and Weyl semimetals [44–46]. The optical properties of TNRSMs have also attracted a lot of interest very recently. Optical conductivity of clean and dirty TNRSMs has been studied with both isotropic and anisotropic models [47–49]. In the absence of a magnetic field, it is shown that the optical conductivity starts a weak and smooth rise at frequency proportional to the radius [48,49]. Therefore, this makes it hard to accurately determine the radius of the nodal ring by the optical conductivity in experiments. The effects of tilt and Dupin cyclide Fermi surface on its optical conductivity have been also explored [50]. The longitudinal magneto-optical conductivity perpendicular to the magnetic field in clear limit with chemical potential localized at the nodal ring plane displays the signature of TNRSMs in the locations of peaks in the optical spectrum [51,52]. However, this signature in experiment is too weak to determine its radius definitely.

In this work we propose a magneto-optical method to determine the radius of TNRSM accurately. By applying a

*czhang@uow.edu.au

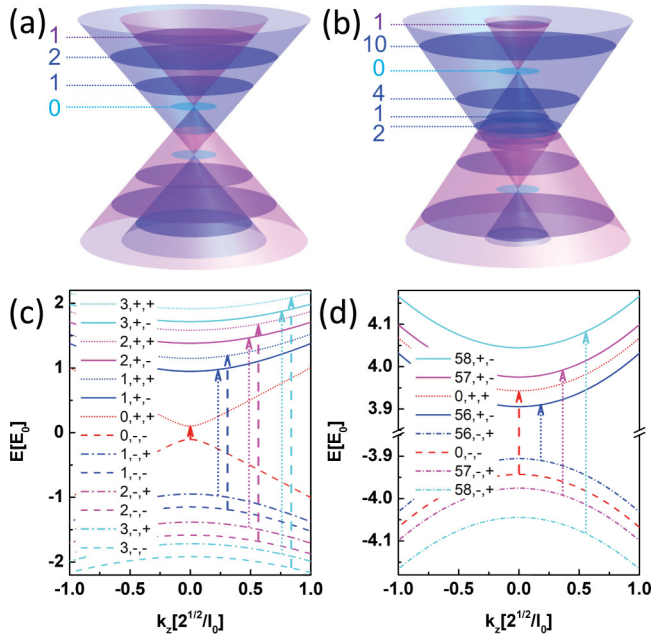

FIG. 1. (a) and (b) The schematic diagrams of the spectra without magnetic field and the LL spectra at $k_z = 0$ with (a) $b_0/\sqrt{B} < 1$ and (b) $b_0/\sqrt{B} > 1$, respectively. The dispersive LL spectra and optical selection rules with (c) $b_0 = 0.1$ and (d) $b_0 = 3.943$, respectively. The index (n, λ, s) for each LL is shown in the legends. The $(n, \lambda, s) = (n, +, +)$, $(n, +, -)$, $(n, -, +)$, and $(n, -, -)$ are labeled as dotted, solid, dot-dashed, and dashed lines, respectively. The allowed transitions between LLs are shown schematically for $\mathrm{Re}(\sigma_{zz})$, in which the transition $L_{n,-,-s} \to L_{n,+,s}$ are labeled for dashed and dotted lines for $s = +$ and $s = -$, respectively. $B = 1.1$ and $\mu = 0$.

uniform magnetic field parallel to the ring axis, which is taken as the z axis, we calculate the axial magneto-optical response σ_{zz}. We shall show that, at the neutral condition (i.e., chemical potential is zero), there exists a resonant peak in σ_{zz} at frequency $2b$, which is determined by the TNRSM radius and is independent of the strength of the magnetic field. Unlike the weak dip found in the in-ring-plane component of magneto-optical response (σ_{xx}) [51], the b-correlated resonant response in the σ_{zz} represents the strongest response which is robust at finite temperature and under finite scattering. In the case of small b the peak height is many times greater than any other inter-Landau level (LL) transition peaks. Apart from this unique B-independent resonance, resonant transitions in σ_{zz} involving higher LLs exhibit double peaks structure. This result shows that the σ_{zz} can be used to determine b easily and accurately. It is interesting to notice that there is a reversal of LLs if b is larger than the magnetic energy. In this case the $n = 0$ transition occurs at higher energy. The location of the $n = 0$ transition remains independent of the magnetic field and the strength is similar strength with those from $n \neq 0$ transitions. The completely different characteristics of σ_{zz} and σ_{xx} are a result of different selection rules governing the quantum magnetic transitions along the ring axis and in the ring plane.

II. FORMALISM

In the presence of the uniform external magnetic field $\mathbf{B} = \bar{B}\mathbf{e}_z$ along z direction, by the standard minimal coupling procedure, the low energy effective Hamiltonian for a TNRSM is given by a 4×4 matrix [2,15]

$$H = v_F \tau_x \otimes (\boldsymbol{\sigma} \cdot \boldsymbol{\pi}) + b\tau_z \otimes \sigma_z, \tag{1}$$

where $\boldsymbol{\pi} = \mathbf{p} + e\mathbf{A}$, $-e$ is the electron charge, $\mathbf{A} = (0, \bar{B}x, 0)$ is the vector potential in Landau gauge, v_F is the Fermi velocity, $\mathbf{p} = (p_x, p_y, p_z)$ is the momentum, $b/\hbar v_F$ is the radius of the nodal ring, and $\boldsymbol{\sigma} = (\sigma_x, \sigma_y, \sigma_z)$ and (τ_x, τ_y, τ_z) are the Pauli matrices for two isospin degree of freedom corresponding to, e.g., spin, sublattices, or atom orbital. We have ignored the effect of external Zeeman splitting.

The eigenvalues are

$$E_{n,\lambda,s}(k_z) = \lambda\sqrt{k_z^2 + (\sqrt{Bn} + \lambda s b_0)^2}, \tag{2}$$

where $\lambda = \pm$, $s = \pm$ and $n = 0, 1, 2, \ldots$, especially when $n = 0$, there is no harm to define $s \equiv \lambda$ for convenience, the energy $E_{n,\lambda,s}(k_z)$ is in unit of $E_0 = \sqrt{2}\hbar v_F/l_0$, $b_0 = b/E_0$, k_z is in unit of $\sqrt{2}/l_0$ with the length $l_0 = \sqrt{\hbar B/e\bar{B}}$, and $\bar{B} = B[T]$. The corresponding eigenstates are given as

$$|n, \lambda, s, k_y, k_z\rangle = \frac{e^{ik_y y + ik_z z}}{\sqrt{L_y L_z \Xi}} c_n \begin{pmatrix} k_z|n-1\rangle \\ (\sqrt{Bn} + \lambda s b_0 - \lambda s E_{n,\lambda,s})|n\rangle \\ -(\lambda s\sqrt{Bn} + b_0 - E_{n,\lambda,s})|n-1\rangle \\ \lambda s k_z|n\rangle \end{pmatrix}, \tag{3}$$

where $c_n = 1$ for $n = 0$ and $1/\sqrt{2}$ for $n > 0$, $\Xi = k_z^2 + (\sqrt{Bn} + \lambda s b_0 - \lambda s E_{n,\lambda,s})^2$, and

$$\langle \mathbf{r}|n, k_y, k_z\rangle = \frac{i^n e^{-(x - k_y B l_0^2)^2/(2Bl_0^2)}}{(2^n n!\sqrt{\pi B} l_0)^{1/2}} H_n\left[\left(x - k_y B l_0^2\right)/\sqrt{B} l_0\right],$$

H_n is the Hermite polynomial. These LLs are dispersive (in k_z) as shown in Fig. 1. The structure of these LLs will control the shape of the dynamical conductivity, as we will elaborate on later.

The magneto-optical conductivity can be obtained by using the Kubo formula,

$$\begin{aligned}\sigma_{uv}(\omega) &= \frac{-i\hbar}{L_x L_y L_z} \sum_{\alpha,\beta} \frac{[f_F(E_\alpha) - f_F(E_\beta)]\langle\alpha|j_u|\beta\rangle\langle\beta|j_v|\alpha\rangle}{(E_\alpha - E_\beta)(E_\alpha - E_\beta + \hbar\omega + i\Gamma)} \\ &= \frac{-i\hbar}{L_x L_y L_z} \frac{[f_F(E_{0,+,+}) - f_F(E_{0,-,-})]\langle 0,+,+|j_u|0,-,-\rangle\langle 0,-,-|j_v|0,+,+\rangle}{(E_{0,+,+} - E_{0,-,-})(E_{0,+,+} - E_{0,-,-} + \hbar\omega + i\Gamma)} \\ &\quad + \frac{-i\hbar}{L_x L_y L_z} \sum_{\alpha,\beta,n\neq 0} \frac{[f_F(E_\alpha) - f_F(E_\beta)]\langle\alpha|j_u|\beta\rangle\langle\beta|j_v|\alpha\rangle}{(E_\alpha - E_\beta)(E_\alpha - E_\beta + \hbar\omega + i\Gamma)},\end{aligned} \tag{4}$$

where $\alpha, \beta = (n, \lambda, s, k_y, k_z)$, $u, v = (x, y, z)$, $f_F(E_\alpha) = 1/[e^{(E_\alpha-\mu)/T} + 1]$ is the Fermi-Dirac distribution with the chemical potential μ and at the temperature T, Γ represents the impurity scattering rate (in this paper, we assume the same Γ for all LLs for simplicity), and the current operators j_u are given by $j_u = ev_F\tau_x \otimes \sigma_u$.

In the clean limit the scattering rate $\Gamma \to 0$ with $\mu = 0$, the optical conductivity is obtained analytically:

$$\mathrm{Re}[\sigma_{zz}(\omega/E_0)]/(e^2/hl_0) = B\sum_{n,s} 2\sqrt{2}\tanh(\omega/4T) \times \frac{(\sqrt{Bn} - sb_0)^2\Theta[(\omega/E_0)^2 - 4(\sqrt{Bn} - sb_0)^2]}{(\omega/E_0)^2\sqrt{(\omega/E_0)^2 - 4(\sqrt{Bn} - sb_0)^2}}. \quad (5)$$

In this work we only focus on the contribution of inter-LL transitions to the conductivity tensor.

III. NUMERICAL RESULTS

The schematic diagrams of spectra are shown in Fig. 1 with (a) $b_0/\sqrt{B} < 1$ and (b) $b_0/\sqrt{B} > 1$ at $k_z = 0$, respectively. Considering the conduction band, i.e., $\lambda = +$, in the case of $b_0/\sqrt{B} < 1$, the LLs are normally ordered and energy increases with n as shown in Fig. 1(a). In the case of $b_0/\sqrt{B} > 1$ [Fig. 1(b)], the LLs in the $s = +$ branch are still normally ordered. However, for the $s = -$ branch there exist two regimes: (i) for small n, $n < b_0^2/B$, the LLs are reversely ordered and energy decreases with n, and (ii) once $n > b_0^2/B$ the LLs resume the normally ordered structure, shown in Fig. 1(b). The structure of these LLs will control the shape of the magnetic optical response parallel to B and the ring axes. Figures 1(c) and 1(d) show the LLs (n, λ, s) spectra at $k_z = 0$ for $b_0 = 0.1$ and 3.943 with $B = 1.1$ and chemical potential $\mu = 0$, respectively. The isospin index $s = \pm$. Generally with $k_z \neq 0$ the LLs do not possess $s = +$ or $s = -$ purely due to strong coupling between isospin σ and τ which leads to the mixture of different isospin components in the wave functions.

Due to the optical selection rule, $\mathrm{Re}(\sigma_{zz})$ only contains transitions between the LLs with the same indices n and opposite isospin s. The optical selection rules which originate from the velocity matrix elements are summarized in Table I and shown schematically in Figs. 1(c) and 1(d). Due to the divergence in density of state at $k_z = 0$, $\mathrm{Re}(\sigma_{zz})$ contains a series of asymmetry resonant peaks appearing at $\omega = 2|\sqrt{Bn} + sb_0|E_0$ as shown in Figs. 2(a) and 2(c). Each strong peak begins with a vertical jump and then decreases with ω due to the three-dimensional (3D) dispersive LL

TABLE I. Optical selection rules.

		Transitions ($k_z = 0$)	Peaks in $\mathrm{Re}(\sigma_{zz})$
$b_0 = 0$	$n = 0$	forbidden	none
	$n \neq 0$	$-\sqrt{Bn} \to \sqrt{Bn}$	$2\sqrt{Bn}$
$b_0 \neq 0$	$n = 0$	$-b_0 \to b_0$	$2b_0$
	$n \neq 0$	$-\lvert\sqrt{Bn} + b_0\rvert \to \lvert\sqrt{Bn} + b_0\rvert$	$2\lvert\sqrt{Bn} + b_0\rvert$
		$-\lvert\sqrt{Bn} - b_0\rvert \to \lvert\sqrt{Bn} - b_0\rvert$	$2\lvert\sqrt{Bn} - b_0\rvert$

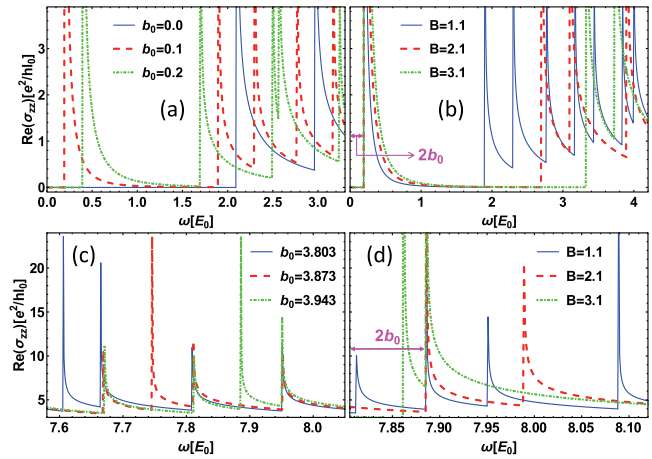

FIG. 2. The plot of $\mathrm{Re}(\sigma_{zz})$ as a function of frequency with $\mu = 0$ for different values of b_0 (a) and (c), and for different values of B (b) and (d). (a) and (b) Normal ordered bands $b_0/B < 1$. (c) and (d) Reverse ordered bands $b_0/B > 1$. In (a) and (c) $B = 1.1$. In (b) $b_0 = 0.1$. In (d) $b_0 = 3.943$. The temperature is $T = 0.01E_0$ and $\Gamma \to 0$.

structures. On the other hand, when $\lambda' = -\lambda$ and $s' = s$, the LL transition is forbidden. In $\mathrm{Re}(\sigma_{zz})$ there is a distinct peak due to $L_{(0,-,-)} \to L_{(0,+,+)}$ transition. The position of this peak is fixed at $2b_0E_0$ under any magnetic field as shown in Figs. 2(b) and 2(d). This peak position determines the ring radius in a definite way. For higher LLs, there is a splitting in the $L_{(n,-,s)} \to L_{(n,+,s)}$ transition. The size of the splitting is fixed at $4b_0E_0$ independent of the magnetic field in normal ordered LLs and is proportional to B for reverse ordered LLs. This provides another method to determine b_0.

Now we analyze the mangeto-optical response when the magnetic field is weak. In this case there is a reversal of band ordering for those LLs with $Bn < b_0^2$, shown in Figs. 1(b) and 1(d). Figures 2(c) and 2(d) show $\mathrm{Re}(\sigma_{zz})$. The $n = 0$ peak is no longer at the lowest energy but its position is still fixed at $2b_0E_0$ independent of the magnetic field. For higher LLs, the distance between the splitted peaks is B dependent $4\sqrt{Bn}E_0$. In Fig. 1(d), only the transitions $-|\sqrt{Bn} - b_0| \to |\sqrt{Bn} - b_0|$ are shown which correspond to the conductivity peaks of $2|\sqrt{Bn} - b_0|$ in Fig. 2(d) with $B = 1.1$ for $n = 56, 0, 57$, and 58, respectively.

In the limit of $b_0 = 0$ we recover the result of Dirac semimetals. In this case there is no $n = 0$ peak, as shown in Fig. 2(a). Considering the massless Dirac fermion as two sets of Weyl fermions with opposite chirality, our results are in good accordance with previous optical conductivity in Weyl semimetal [44]. Comparing with the case of Dirac semimetals, i.e., $b_0 = 0$, $\mathrm{Re}(\sigma_{zz})$ of TNRSM probes a more complex set of magnetic transitions which is completely different from that probed by $\mathrm{Re}(\sigma_{xx})$ as shown in Refs. [51,52]. The magneto-optical response along and perpendicular to the ring axis are governed by completely different selection rules. It should also be noted that the nodal ring considered here is intrinsic, i.e., b is finite in the absence of the magnetic field [2,15,48,49]. The ring in Refs. [51,52] is induced by the magnetic field and b is proportional to the applied magnetic field. Under a finite chemical potential the optical conductivity

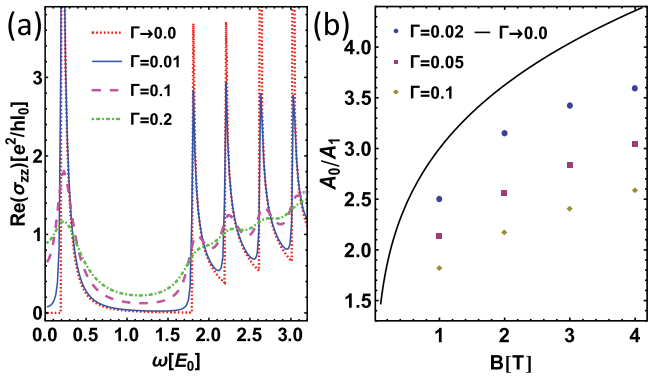

FIG. 3. (a) The plot of $\mathrm{Re}(\sigma_{zz})$ as a function of frequency for several values of scattering rate (in unit of E_0) with $B = 1$, and $T = 0.01E_0$. (b) The ratio of the amplitude of $\mathrm{Re}(\sigma_{zz})$ peaks between the zeroth LL and the first LL. The black solid line shows the analytical results for $\Gamma \to 0$ and $T \to 0$. The dots show the numerical results with several values of scattering rate (in unit of E_0) and $T = 0.01E_0$. $b_0 = 0.1$ and $\mu = 0$.

becomes zero for $\omega < 2\mu$. The characteristics for $\omega > 2\mu$ is independent of the chemical potential.

Figures 2(b) and 2(d) show the magnetic field dependence of $\mathrm{Re}(\sigma_{zz})$ for (b) $b_0 = 0.1$ and (d) $b_0 = 3.943$ with $\mu = 0$, and $T = 0.01E_0$ in clean limit $\Gamma \to 0$, respectively. The $n = 0$ peak located at $\omega = 2b_0E_0$ is unaffected by the strength of the magnetic field, while the other double peaks at $\omega = 2|\sqrt{Bn} + sb_0|E_0$ for $n \geqslant 1$ LLs are shifted by the magnetic field. For $n \geqslant 1$ LLs, in the case $Bn \geqslant b_0^2$ as shown in Figs. 1(c) and 2(a), the distance between the splitted peaks for finite n is $4b_0E_0$.

The B-independent peak position in $\mathrm{Re}[\sigma_{zz}(\omega)]$ is robust and fixed in the presence of finite scattering. Here we include the scattering effect phenomenologically by considering a finite scattering rate Γ. For $\Gamma = 0.01E_0$, $0.1E_0$, and $0.2E_0$, we can obtain the conductivity numerically, shown in Fig. 3(a) with temperature $T = 0.01E_0$, $b_0 = 0.1$, and $B = 1$ at chemical potential $\mu = 0.0$. The finite impurity scattering mainly tends to blur out the resonant peaks and the oscillations are still well defined for $\Gamma = 0.2E_0$ for $\mathrm{Re}(\sigma_{zz})$. For a Fermi velocity of $v_F \sim 10^5$ m/s, this corresponds to a scattering rate of $\Gamma \sim 0.72$ meV.

Now we estimate the ratio of the amplitude of the B-independent resonance to that of the neighboring resonance. For $\mu = 0$ and $b_0 = 0.1$, neighboring resonance is at $n = 1$. At $n = 0$, $\omega/E_0 \to 2b_0$, and $T \to 0$, $\mathrm{Re}[\sigma_{zz}(\omega/E_0)]/(e^2/hl_0) \to (B/2\sqrt{2}\sqrt{b_0})[\Theta(\omega/E_0 - 2b_0)/\sqrt{(\omega/E_0 - 2b_0)}]$ and define $A_0 = B/2\sqrt{2}\sqrt{b_0}$. Similarly at $n = 1$, $s = -$, $\omega/E_0 \to 2|\sqrt{B} - b_0|$, and $T \to 0$, $\frac{\mathrm{Re}[\sigma_{zz}(\omega/E_0)]}{e^2/hl_0} \to \frac{B}{2\sqrt{2}\sqrt{|\sqrt{B}-b_0|}} \frac{\Theta(\omega/E_0+2b_0-2\sqrt{B})}{\sqrt{(\omega/E_0+2b_0-2\sqrt{B})}}$ and define $A_1 = B/2\sqrt{2}\sqrt{|\sqrt{B} - b_0|}$. We obtain the ratio of the peaks, given as

$$A_0/A_1 = \sqrt{|\sqrt{B} - b_0|/b_0}, \tag{6}$$

which are shown by the black line in Fig. 3(b) for $b_0 = 0.1$. For $B > 1$, the amplitude A_0 is many times of magnitude greater than A_1. At finite temperature and finite scattering, A_0 is still stronger than A_1, shown in Fig. 3(b). The strongest A_0 is ideal for experimental detection of b_0. In the case that LLs are reversed, $b_0 = 3.943$, the neighboring resonance is at finite n. In this case the ratio increases as the magnetic field decreases. At very weak magnetic field, the amplitude B-independent resonance is the same as that of the neighboring resonance. Therefore the $n = 0$ transition still represents the strong enough signal suitable for determining b_0.

IV. DISCUSSION AND CONCLUSION

We estimate the relevant frequency of the optical field. We take the material candidate CaAgAs [4] as a concrete example. Considering the Fermi velocity in the order of 10^5 ms^{-1}, it can be estimated that $E_0 \sim 3.6$ meV. For $b_0 \sim 18$, we get the frequency $\omega \sim 1.58 \times 10^{13}$ Hz. The frequency of the laser lies in the region of 10^{13} Hz. This is very close to a technologically important and scientifically unexplored terahertz window.

It should be noted that our result is applicable to the types of TNRSMs whose electronic properties are governed by the model Hamiltonian Eq. (1). This four-band model describes certain types of TNRSMs. Equation (1) is not a general model for all TNRSMs. As mentioned below, there exists other TNRSMs described by different models. Our results will also be altered in a TNRSMs system where a finite gap exists. With our model, the result of accurately determining b obtained in this work is valid as long as the quantum states used in calculating σ_{zz} are accurate. The linear model given by Eq. (1) is a type of low energy effective model. The region for this model to be valid is finite, say ΔE_L. The energies of high n LLs can exceed this region and σ_{zz} can become inaccurate. Our central results of the B-independent resonance is due to the $n = 0$ LL from the valence and the conduction band with opposite isospins. The $n = 0$ LL is the most accurate state for any ΔE_L. For this reason, our central result remains accurate and valid. Some other transitions involving higher LL can be less accurate if the LL energy exceeds ΔE_L. It has been shown that the linear model is valid in an energy window of more than 200 meV i.e., $(-100$ meV, 100 meV) as confirmed in Fig. 4 in Ref. [53] and Table 7 in Ref. [12]. This linear region can include up to 100 LLs for $B = 1$ T. There exists a different type of TNRSMs which is formed by inverted band [10,11,54]. This type of nodal ring is described by a two-band model $H = \frac{-\hbar^2}{2m}(k_x^2 + k_y^2 - b^2)\tau_x + \hbar v_F k_z \tau_z$. In this nodal ring system, the region of linear dispersion is very narrow. The LL structure for this nodal is completely different to that in the nodal ring used in our study.

Finally, we would like to mention that Eq. (1) is a low energy effective Hamiltonian. Within this model, the radius of the ring is b. If the band deviates from the linear dispersion at high energy, $n = 0$ state will not be affected and the B-independent resonant transition remains accurate. However, the position of the ring may be at the nonlinear part of the energy dispersion. In this case the ring radius is not exactly b but is a unique function of b. This unique function can be derived once the band dispersion at the ring position is known.

In summary, we studied the axial magneto-optical conductivity $\mathrm{Re}(\sigma_{zz})$ of TNRSM. We found that when the magnetic field is along the nodal ring axis, the response along the axis exhibits two distinctive features: (i) There exists a resonant

peak from $n = 0$ transition. The resonant position is independent of the magnetic field and is fixed at $2b$ for both the normal ordered LL bands and reverse ordered LL bands. The amplitude of this distinct resonance is many times stronger than that of any other transitions for normal ordered LL bands and is similar strength for reverse ordered LL bands. This unique resonance provides the most suitable probe for determining the radius of TNRSM. (ii) For transitions from higher LLs, the peaks split. The splitting is $4b$ independent of the magnetic field in normal ordered LLs and is proportional to B for reverse ordered LLs. The origin of these distinctive features is the orientation dependent optical selection rules. The $\mathrm{Re}(\sigma_{zz})$ is governed by selection rules different from those quantum magnetic transitions in $\mathrm{Re}(\sigma_{xx})$. We expect that our result will facilitate experimental studies to characterize TNRSM, for example to determine the radius of TNRSM. The significant advantage of the current result is that the quantity we proposed to determine the ring radius, the $n = 0$ resonance in $\mathrm{Re}[\sigma_{zz}(\omega)]$, is independent of the B field. As a result b can be accurately determined under a very weak magnetic field. Apart from a high magnetic field normally required for the quantum Hall effect, a toroidal field is necessary to determine b [23]. The orbit magnetization also requires a strong magnetic field [27] to induce a measurable magnetization.

ACKNOWLEDGMENTS

The work is supported by the Australian Research Council (Grant No. DP160101474), NSFC (Grant No. 11774006), and NBRP of China (Grant No. 2012CB921300).

[1] T. T. Heikkilä and G. E. Volovik, Pisma Zh. Eksp. Teor. Fiz. **93**, 63 (2011); JETP Lett. **93**, 59 (2011).
[2] A. A. Burkov, M. D. Hook, and L. Balents, Phys. Rev. B **84**, 235126 (2011).
[3] L. M. Schoop, M. N. Ali, C. Straßer, A. Topp, A. Varykhalov, D. Marchenko, V. Duppel, S. S. P. Parkin, B. V. Lotsch, and C. R. Ast, Nat. Commun. **7**, 11696 (2016).
[4] D. Takane, K. Nakayama, S. Souma, T. Wada, Y. Okamoto, K. Takenaka, Y. Yamakawa, A. Yamakage, T. Mitsuhashi, K. Horiba, H. Kumigashira, T. Takahashi, and T. Sato, npj Quantum Mater. **3**, 1 (2018).
[5] C.-K. Chiu, J. C. Y. Teo, A. P. Schnyder, and S. Ryu, Rev. Mod. Phys. **88**, 035005 (2016).
[6] M. Z. Hasan, S.-Y. Xu, I. Belopolski, and S.-M. Huang, Annu. Rev. Condens. Matter Phys. **8**, 289 (2017).
[7] B. Yan and C. Felser, Annu. Rev. Condens. Matter Phys. **8**, 337 (2017).
[8] N. Armitage, E. Mele, and A. Vishwanath, Rev. Mod. Phys. **90**, 015001 (2018).
[9] R. Yu, Z. Fang, X. Dai, and H. Weng, Front. Phys. **12**, 127202 (2017).
[10] C. Fang, Y. Chen, H.-Y. Kee, and L. Fu, Phys. Rev. B **92**, 081201(R) (2015).
[11] C. Fang, H. Weng, X. Dai, and Z. Fang, Chin. Phys. B **25**, 117106 (2016).
[12] S.-Y. Yang, H. Yang, E. Derunova, S. S. P. Parkin, B. Yan, and M. N. Ali, Adv. Phys. X **3**, 1414631 (2018).
[13] Y. Kim, B. J. Wieder, C. L. Kane, and A. M. Rappe, Phys. Rev. Lett. **115**, 036806 (2015).
[14] Y.-H. Chan, C.-K. Chiu, M. Y. Chou, and A. P. Schnyder, Phys. Rev. B **93**, 205132 (2016).
[15] M. Koshino and I. F. Hizbullah, Phys. Rev. B **93**, 045201 (2016).
[16] C. Li, C. M. Wang, B. Wan, X. Wan, H.-Z. Lu, and X. C. Xie, Phys. Rev. Lett. **120**, 146602 (2018).
[17] H. Yang, R. Moessner, and L.-K. Lim, Phys. Rev. B **97**, 165118 (2018).
[18] L. Oroszlány, B. Dóra, J. Cserti, and A. Cortijo, Phys. Rev. B **97**, 205107 (2018).
[19] J. Hu, Z. Tang, J. Liu, X. Liu, Y. Zhu, D. Graf, K. Myhro, S. Tran, C. N. Lau, J. Wei, and Z. Mao, Phys. Rev. Lett. **117**, 016602 (2016).
[20] M. R. van Delft, S. Pezzini, T. Khouri, C. S. A. Müller, M. Breitkreiz, L. M. Schoop, A. Carrington, N. E. Hussey, and S. Wiedmann, Phys. Rev. Lett. **121**, 256602 (2018).
[21] S. Li, Z. Guo, D. Fu, X.-C. Pan, J. Wang, K. Ran, S. Bao, Z. Ma, Z. Cai, R. Wang, R. Yu, J. Sun, F. Song, and J. Wen, Sci. Bull. **63**, 535 (2018).
[22] J.-W. Rhim and Y. B. Kim, Phys. Rev. B **92**, 045126 (2015).
[23] K. Mullen, B. Uchoa, and D. T. Glatzhofer, Phys. Rev. Lett. **115**, 026403 (2015).
[24] A. A. Burkov, Phys. Rev. B **97**, 165104 (2018).
[25] H. Jiang, L. Li, J. Gong, and S. Chen, Eur. Phys. J. B **91**, 75 (2018).
[26] W. Chen, K. Luo, L. Li, and O. Zilberberg, Phys. Rev. Lett. **121**, 166802 (2018).
[27] S. T. Ramamurthy and T. L. Hughes, Phys. Rev. B **95**, 075138 (2017).
[28] T. Rauch, H. Nguyen Minh, J. Henk, and I. Mertig, Phys. Rev. B **96**, 235103 (2017).
[29] M. Biderang, A. Leonhardt, N. Raghuvanshi, A. P. Schnyder, and A. Akbari, Phys. Rev. B **98**, 075115 (2018).
[30] V. I. Gavrilenko, A. A. Perov, A. P. Protogenov, R. V. Turkevich, and E. V. Chulkov, Phys. Rev. B **97**, 115204 (2018).
[31] W. B. Rui, Y. X. Zhao, and A. P. Schnyder, Phys. Rev. B **97**, 161113(R) (2018).
[32] R. A. Molina and J. González, Phys. Rev. Lett. **120**, 146601 (2018).
[33] D. A. Khokhlov, A. L. Rakhmanov, and A. V. Rozhkov, Phys. Rev. B **97**, 235418 (2018).
[34] Y. Sun, Y. Zhang, C.-X. Liu, C. Felser, and B. Yan, Phys. Rev. B **95**, 235104 (2017).
[35] B. Roy, Phys. Rev. B **96**, 041113(R) (2017).
[36] J. Liu and L. Balents, Phys. Rev. B **95**, 075426 (2017).
[37] A. P. Schnyder and S. Ryu, Phys. Rev. B **84**, 060504(R) (2011).
[38] R. Nandkishore, Phys. Rev. B **93**, 020506(R) (2016).
[39] Y. Wang and R. M. Nandkishore, Phys. Rev. B **95**, 060506(R) (2017).
[40] S. E. Han, G. Y. Cho, and E.-G. Moon, Phys. Rev. B **95**, 094502 (2017).

[41] S. A. Yang, H. Pan, and F. Zhang, Phys. Rev. Lett. **113**, 046401 (2014).
[42] S.-Y. Xu, I. Belopolski, N. Alidoust, M. Neupane, G. Bian, C. Zhang, R. Sankar, G. Chang, Z. Yuan, C.-C. Lee, S.-M. Huang, H. Zheng, J. Ma, D. S. Sanchez, B. K. Wang, A. Bansil, F. Chou, P. P. Shibayev, H. Lin, S. Jia, and M. Z. Hasan, Science **349**, 613 (2015).
[43] A. A. Burkov, Phys. Rev. Lett. **113**, 187202 (2014).
[44] P. E. C. Ashby and J. P. Carbotte, Phys. Rev. B **87**, 245131 (2013).
[45] Y. Sun and A.-M. Wang, Phys. Rev. B **96**, 085147 (2017).
[46] J. D. Malcolm and E. J. Nicol, Phys. Rev. B **94**, 224305 (2016).
[47] S. Barati and S. H. Abedinpour, Phys. Rev. B **96**, 155150 (2017).
[48] J. P. Carbotte, J. Phys.: Condens. Matter **29**, 045301 (2017).
[49] S. P. Mukherjee and J. P. Carbotte, Phys. Rev. B **95**, 214203 (2017).
[50] S. Ahn, E. J. Mele, and H. Min, Phys. Rev. Lett. **119**, 147402 (2017).
[51] R. Y. Chen, Z. G. Chen, X.-Y. Song, J. A. Schneeloch, G. D. Gu, F. Wang, and N. L. Wang, Phys. Rev. Lett. **115**, 176404 (2015).
[52] Y.-X. Wang, Eur. Phys. J. B **90**, 99 (2017).
[53] M. A. Zeb and H.-Y. Kee, Phys. Rev. B **86**, 085149 (2012).
[54] Z. Yan, P.-W. Huang, and Z. Wang, Phys. Rev. B **93**, 085138 (2016).